RSC Advances

PAPER

View Article Online
View Journal | View Issue

Cite this: *RSC Adv.*, 2026, **16**, 27818

Covalently silane-bridged e-graphene oxide nanosheets toward year-long dispersion-stable epoxy nanocomposites with superior corrosion protection

Anh-Tuan Pham,*[ab] Quan-Doan Mai,*[a] Ngo Thi Loan,[ab] Nguyen Thai Huy,[ab] Ngo Thi Phuong Anh,[b] Pham Cong Thanh,[ce] Nguyen Thi Trang,[be] Le Minh Quang,[b] Nguyen Van Quyet,[b] Ta Ngoc Bach[d] and Anh-Tuan Le*[a]

Epoxy resins are extensively used in protective coating applications owing to their excellent adhesion, mechanical strength, and chemical resistance; however, maintaining these properties under prolonged service environments remains challenging. Although nanoscale fillers have been widely explored to enhance the durability of epoxy coatings, the long-term dispersion stability of nanofillers in epoxy matrices remains severely limited by interfacial incompatibility and aggregation. In this work, electrochemically synthesized graphene oxide (e-GO) nanosheets are successfully prepared in an aqueous environment, with intrinsically abundant oxygen-containing functional groups. By carefully selecting silane molecules with high chemical compatibility toward epoxy, a covalent silane-bridging (CSB) strategy is established to chemically integrate e-GO nanosheets into the epoxy matrix, enabling strong interfacial compatibility and long-term dispersion stability. As a result, the epoxy/CSB-eGO nanocomposites exhibit exceptional dispersion stability exceeding one year without observable aggregation, together with simultaneous enhancements in mechanical performance and corrosion resistance. At an optimized CSB-eGO loading of 0.5 wt%, the tensile and flexural strengths are enhanced by 26% and 43%, respectively, while the impact strength increases by 36% at a low loading of 0.1 wt%. Electrochemical impedance spectroscopy further demonstrates outstanding corrosion resistance at an optimized CSB-eGO loading of 1.0 wt%, with the pore resistance (R_{pore}) increasing from 8488 Ω for pristine epoxy to 2.46 × 10^5 Ω, corresponding to an approximately 30-fold enhancement. This work provides a scalable strategy for developing durable epoxy nanocomposite coatings with long-term mechanical reliability and corrosion protection.

Received 19th March 2026
Accepted 15th May 2026

DOI: 10.1039/d6ra02282k

rsc.li/rsc-advances

1. Introduction

Epoxy resins are among the most widely used matrix materials for protective coating applications owing to their excellent adhesion to various substrates, high mechanical integrity, and good resistance to chemicals and corrosive environments.[1–3] These attributes make epoxy coatings particularly attractive for corrosion protection in industrial, marine, and infrastructure applications. However, under prolonged service conditions involving moisture, salt exposure, and thermal fluctuations, the long-term reliability of epoxy coatings remains a critical concern.[4,5] Water uptake, microcrack formation, and gradual degradation of the epoxy polymer network can progressively compromise the barrier properties and mechanical integrity of epoxy coatings, ultimately leading to the loss of effective corrosion protection. Consequently, while epoxy coatings often exhibit satisfactory initial performance, maintaining their mechanical and anti-corrosive functions over extended service periods remains a fundamental challenge.[6,7] Therefore, enhancing the mechanical robustness and durability of epoxy resins has long been recognized as a critical requirement to meet increasingly demanding service conditions. Over the past several decades, a wide range of reinforcement strategies have been developed and demonstrated to improve the performance of epoxy systems.[8] From a materials design perspective, these strategies can generally be classified into *in situ* and *ex situ*

[a]*Phenikaa University Nano Institute (PHENA), Phenikaa School of Engineering (PSE), Phenikaa University, Hanoi 12116, Vietnam. E-mail: fattuan@phenikaa-uni.edu.vn; doan.maiquan@phenikaa-uni.edu.vn; tuan.leanh@phenikaa-uni.edu.vn*

[b]*Faculty of Biotechnology, Chemistry and Environmental Engineering, Phenikaa School of Engineering (PSE), Phenikaa University, Hanoi 12116, Vietnam*

[c]*Faculty of Materials Science and Engineering (MSE), Phenikaa School of Engineering (PSE), Phenikaa University, Hanoi 12116, Vietnam*

[d]*Institute of Materials Science (IMS), Vietnam Academy of Science and Technology, 18 Hoang Quoc Viet, Hanoi 10000, Vietnam*

[e]*Vicostone Joint Stock Company & Phenikaa Chemicals Factory, Phenikaa Group, Hoa Lac High-Technology Industrial Zone, Hanoi 10000, Vietnam*

approaches.[9,10] Compared with *in situ* modification, *ex situ* incorporation of reinforcement fillers into commercially available epoxy systems is more practical and industrially compatible. However, the effectiveness of *ex situ* reinforcement is often severely limited by poor dispersion stability and weak interfacial compatibility, as physically blended additives are prone to aggregation, phase separation, and interfacial degradation over time.[11–15] Consequently, achieving stable nano-dispersion together with durable nano–epoxy interfacial integration remains a major challenge for high-performance epoxy coatings.

Ex situ modification of epoxy resins has traditionally relied on the incorporation of a broad spectrum of organic and inorganic additives to tailor mechanical and durability-related properties. Among these, liquid rubbers and elastomeric modifiers represent one of the earliest and most extensively studied toughening strategies.[16,17] The incorporation of rubbery phases can effectively improve fracture toughness and impact resistance by promoting energy dissipation mechanisms such as cavitation and shear banding. However, these modifiers typically induce a pronounced reduction in stiffness, thermal resistance, and chemical durability, which limits their suitability for high-performance protective coating applications.[17] Thermoplastic tougheners constitute another widely adopted class of *ex situ* modifiers, offering improved toughness while better preserving stiffness and thermal stability compared to rubber-based systems.[18] Through phase separation and plastic deformation mechanisms, thermoplastic additives can enhance crack resistance and damage tolerance. Nevertheless, their effectiveness is often constrained by high processing viscosity, phase compatibility issues, and the requirement for relatively high loading levels, which may adversely affect coating processability and barrier performance. Inorganic micro-scale fillers, such as silica, alumina, or mineral particulates, have also been extensively employed to enhance stiffness, wear resistance, and dimensional stability of epoxy coatings.[19,20] These fillers are generally cost-effective and industrially scalable, and they can improve certain barrier properties by increasing diffusion path length. However, their relatively large particle size and low specific surface area limit interfacial interaction with the epoxy matrix, resulting in inefficient stress transfer and marginal improvements in toughness. Moreover, high filler loadings are often required to achieve meaningful reinforcement, which can lead to brittleness, sedimentation, and processing challenges in coating formulations. Collectively, while these conventional *ex situ* additives provide practical and well-established routes for property modification, their performance is often governed by intrinsic trade-offs between toughness, stiffness, processability, and long-term durability. These limitations have driven increasing interest toward alternative reinforcement strategies capable of delivering multifunctional enhancement at low additive content, thereby paving the way for the emergence of nano-scale fillers as next-generation *ex situ* modifiers.

Building upon the limitations of conventional *ex situ* modifiers, nano-scale fillers have emerged as a highly promising class of reinforcement materials for epoxy-based coatings.[21–23] Compared with micro-scale fillers, nanomaterials offer exceptionally high specific surface area and aspect ratio, enabling significant enhancement of mechanical, barrier, and anti-corrosive properties at relatively low loading levels. A wide range of nano-fillers, including silica nanoparticles, layered silicates, carbon nanotubes, and graphene-based materials, have been explored for *ex situ* modification of epoxy systems. When properly dispersed, these nano-fillers can effectively hinder crack initiation and propagation, improve stress transfer efficiency, and markedly increase the tortuosity of diffusion pathways for water, oxygen, and aggressive ions, thereby enhancing both mechanical durability and long-term corrosion resistance. Despite these advantages, the performance of nano-reinforced epoxy coatings is strongly governed by the quality of dispersion and the strength of interfacial interactions between the nano-fillers and the epoxy matrix. Owing to their high surface energy, nano-fillers are inherently prone to agglomeration, which leads to heterogeneous microstructures and the formation of stress concentration sites that deteriorate mechanical integrity and barrier performance.[24,25] Moreover, weak interfacial adhesion limits effective load transfer and accelerates interfacial debonding under moisture exposure, thermal cycling, and mechanical stress, undermining the long-term stability of the coating system. Consequently, achieving uniform dispersion while simultaneously enhancing nano–epoxy interfacial interactions has become a central challenge in the *ex situ* design of high-performance epoxy coatings. The effectiveness of nano-scale reinforcement therefore depends not only on the intrinsic properties of the nanomaterials themselves, but also critically on interfacial engineering strategies that can promote strong physicochemical interactions with the epoxy network, ensuring durable reinforcement under realistic service conditions. Achieving uniform dispersion together with durable nano–epoxy interfacial interactions therefore represents a fundamental bottleneck in the development of long-lasting epoxy nanocomposite coatings.

In recent years, a variety of strategies have been reported to improve nano–epoxy interfacial interactions, including mechanical high-shear processing, ultrasonication,[26] solvent-exchange techniques, non-covalent surfactant or polymer stabilizer wrapping,[27] and covalent surface functionalization.[28,29] Mechanical approaches such as high-shear mixing and ultrasonication have been widely employed due to their simplicity and broad applicability for dispersing nanoparticles, carbon nanotubes, and graphene-based materials in epoxy matrices.[30] For example, Bittmann *et al.* demonstrated that ultrasonication improved the flexural strength of TiO_2/epoxy composites; however, significant nanoparticle aggregation still remained due to insufficient disruption of strong agglomerates.[31] As a result, mechanically induced dispersion remains inherently transient because it does not fundamentally resolve the surface incompatibility between nanofillers and the epoxy matrix. Compared to mechanical dispersion, solvent-exchange strategies have shown improved capability in suppressing irreversible nanoparticle agglomeration during epoxy processing. Mehrabi *et al.* fabricated GO/epoxy nanocomposites *via* a solvent-exchange route and achieved simultaneous improvements in mechanical properties and fracture toughness owing

to improved GO dispersion.[32] Nevertheless, because the intrinsic surface chemistry of GO remained unchanged, the long-term dispersion stability was still inherently limited. In addition, solvent-exchange processes require strict solvent compatibility control, increasing processing complexity and limiting industrial practicality. Surface modification strategies have therefore attracted increasing attention for improving nano–epoxy compatibility. Wei and Inam employed non-covalent surfactant wrapping using sodium dodecyl sulfate (SDS) and gum arabic (GA) to improve graphene dispersion in epoxy matrices, leading to enhanced mechanical performance.[33] Similarly, Javidparvar *et al.* reported a non-covalent functionalization of GO through π–π interactions and electrostatic adsorption involving benzimidazole and cerium species, resulting in significantly improved dispersion and mechanical reinforcement.[34] However, because these stabilization mechanisms are predominantly based on reversible physical adsorption and electrostatic interactions, the long-term dispersion stability and interfacial robustness remain sensitive to environmental exposure and processing conditions. Consequently, recent research has increasingly shifted toward covalent interfacial engineering strategies capable of establishing robust and stable interfaces between nanofillers and epoxy network. Nevertheless, successful covalent functionalization often requires multi-step surface activation and grafting procedures, leading to increased process complexity. For example, Vo *et al.* developed a multi-step covalent modification strategy for montmorillonite-based epoxy nanocomposites involving surface activation, silanization, and polymer grafting steps to achieve sufficient compatibility with epoxy matrices.[35] Therefore, simplifying covalent surface functionalization through nanofiller with intrinsically reactive surfaces together with carefully designed interfacial chemistry remains highly desirable for achieving stable nano-dispersion in epoxy matrices while maintaining practical feasibility for industrial applications.

In this study, electrochemically synthesized graphene oxide (e-GO) nanosheets were successfully prepared in an aqueous environment, yielding e-GO with intrinsically abundant surface functional groups generated directly during the synthesis process. By carefully selecting silane molecules with high compatibility toward epoxy, covalent silane-bridged e-GO nanosheets (CSB-eGO) were successfully fabricated through direct silanization in aqueous media. The resulting CSB-eGO nanosheets exhibited pronounced hydrophobicity and could be directly dispersed into epoxy without the assistance of solvents or intensive mechanical dispersion. Owing to the high density of reactive surface sites together with the optimized covalent interfacial design, the dispersion stability of CSB-eGO within the epoxy matrix could extend to the order of years. As a result, the epoxy/CSB-eGO nanocomposites exhibit markedly enhanced mechanical strength and superior corrosion protection. At an optimized CSB-eGO loading of 0.5 wt%, the tensile and flexural strengths increase by 26% and 39%, respectively, while the impact strength is enhanced by 42% at a low loading of 0.1 wt%. Electrochemical impedance spectroscopy further demonstrates outstanding corrosion resistance at an optimized CSB-eGO loading of 1.0 wt%, with the pore resistance (R_{pore}) increasing from 8488 Ω for pristine epoxy to 2.46×10^5 Ω, corresponding to an approximately 30-fold enhancement. Overall, this work provides a scalable and practical strategy for developing durable epoxy nanocomposite coatings with long-term mechanical reliability and corrosion protection.

2. Experimental section

2.1. Materials

Sulfuric acid (H_2SO_4, 98 wt%), 3-methacryloxypropyltrimethoxysilane ($C_{10}H_{20}O_5Si$, ≥98%), triethylenetetramine (TETA, $C_6H_{18}N_4$, ≥98%) and ethanol (C_2H_5OH, ≥99.7%) were purchased from Shanghai Chemical Reagent Co. and used as received without further purification. The epoxy resin used in this study was a commercially available diglycidyl ether of bisphenol A (DGEBA)-based epoxy (Epotec YD 011X-75). Carbon steel substrates (SS400 grade) were employed for corrosion resistance evaluation. Double-distilled water was used throughout all experiments.

2.2. Synthesis of electrochemical graphene oxide (e-GO) nanosheets (NSs)

In this work, electrochemical graphene oxide (e-GO) nanosheets (NSs) were synthesized *via* an electrochemical exfoliation method using graphite electrodes as both the anode and cathode in a double-distilled water electrolyte containing 0.1 M H_2SO_4, as schematically illustrated in Scheme 1. The two-electrode system was connected to a direct current (DC) power supply with an applied voltage of 10 V, and the electrodes were positioned parallel to each other at a fixed distance of 5 cm. During electrochemical exfoliation, sulfate ions (SO_4^{2-}) from the electrolyte, owing to their suitable ionic size, were intercalated into the stacked graphene layers within the graphite structure, leading to progressive layer separation. Simultaneously, the aqueous environment and the presence of SO_4^{2-} ions facilitated the oxidation of the exfoliated graphene sheets immediately upon their dispersion into the electrolyte, resulting in the formation of oxygen-containing functional groups on the surface of the resulting e-GO NSs. The combined processes of graphite exfoliation and electrochemical oxidation were carried out for 5 h, yielding e-GO NSs with nanometer-scale thickness and large specific surface area. Owing to the hydrophilic surface enriched with oxygen-containing functional groups, the as-prepared e-GO NSs exhibited high dispersibility and excellent colloidal stability in aqueous media, and were directly used in the subsequent surface functionalization step without further purification or modification.

2.3. Synthesis of covalently silane-bridged e-GO nanosheets (CSB-eGO NSs)

The electrochemically exfoliated graphene oxide (e-GO) nanosheets obtained as described above were directly used for surface modification *via* silanization without any intermediate treatment or purification step. The as-prepared aqueous e-GO dispersion exhibited an intrinsic pH of approximately 2 due to

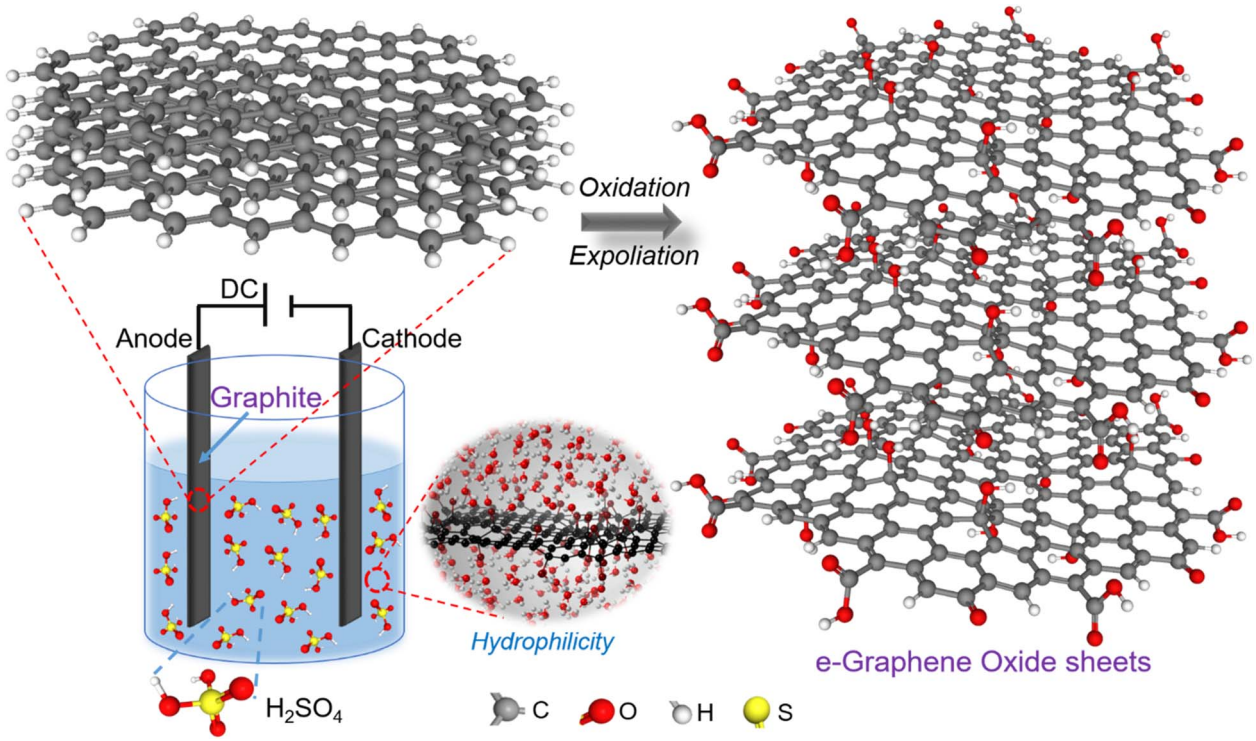

Scheme 1 Schematic illustration of the electrochemical fabrication of hydrophilic e-GO nanosheets (e-GO NSs) in an aqueous medium and their formation mechanism.

the presence of H_2SO_4, which served not only as the electrolyte for graphite exfoliation and oxidation, but also provided an acidic environment favorable for silane hydrolysis during the silanization process. Consequently, no additional pH adjustment or external acid catalyst was required, which simplified the procedure and minimized the potential influence of extraneous chemicals on the colloidal stability of the e-GO nanosheets. In a typical process, 1 L of the e-GO aqueous dispersion was transferred into a 2 L glass beaker and stirred magnetically at 400 rpm to ensure homogeneity. A silane solution with a total volume of 250 mL, consisting of 125 mL of 3-methacryloxypropyltrimethoxysilane (MPTMS) pre-dispersed in 125 mL of ethanol, was then added dropwise into the e-GO dispersion under continuous stirring. The mass ratio of MPTMS to e-GO was optimized and fixed at 1 : 10. The silanization reaction was carried out under optimized conditions: (i) the overall pH of the reaction system was maintained at 2 to ensure controlled silane hydrolysis, which was inherently achieved by the acidic e-GO dispersion generated from the electrochemical exfoliation process; (ii) the reaction temperature was maintained at 70 °C throughout the process using a thermostated magnetic stirrer and monitored every 10 min; and (iii) a constant stirring speed of 400 rpm was applied to promote uniform dispersion of MPTMS and effective contact between the silane molecules and the e-GO nanosheet surfaces. The silanization reaction was allowed to proceed for 8 h. Upon completion of the reaction, the MPTMS-modified e-GO formed a viscous gel-like phase that settled at the bottom of the reaction vessel and spontaneously separated from the aqueous phase, indicating a transition of the nanosheet surface from hydrophilic to hydrophobic character. The supernatant water was readily removed by decantation without material loss, as the surface-modified e-GO nanosheets had fully separated from the aqueous phase. The collected gel-like product was subsequently washed three times with ethanol to remove unreacted or physically adsorbed MPTMS. Finally, the silane-modified e-GO nanosheets were dried at 60 °C for 4 h. The resulting material was denoted as covalently silane-bridged e-GO nanosheets (CSB-eGO NSs).

2.4. Fabrication of epoxy/CSB-eGO nanocomposite coatings

Surface modification *via* covalent silane bridging enables CSB-eGO to be directly dispersed into the epoxy matrix owing to its enhanced interfacial compatibility, without the need for complex or energy-intensive dispersion techniques. Specifically, epoxy/CSB-eGO nanocomposites with different CSB-eGO loadings were prepared by dispersing a predetermined amount of CSB-eGO nanosheets into the epoxy resin through simple mechanical stirring at 200 rpm for 5 min. Subsequently, epoxy/CSB-eGO nanocomposite coatings were formulated by directly incorporating triethylenetetramine (TETA) as the curing agent at a fixed content of 5.0 wt% relative to the epoxy resin. The curing process was carried out at room temperature for 12 h to obtain fully cured epoxy/CSB-eGO nanocomposite coatings.

2.5. Characterization

The morphological characteristics of e-GO NSs were investigated using a field-emission scanning electron microscope (FE-SEM, Hitachi S-4800) operated at an accelerating voltage of 5 kV,

and high-resolution transmission electron microscopy (HR-TEM, JEOL JEM-2100) operated at 200 kV to examine surface morphology and electron transparency. The chemical bonding characteristics and structural composition were analyzed by Raman spectroscopy, conducted using a Horiba Macro-RAM™ spectrometer with a 785 nm laser excitation, and by Fourier transform infrared (FTIR) spectroscopy using a Spectrum Two spectrometer (PerkinElmer) in the wavenumber range of 350–8300 cm^{-1}. The formation of covalent bonds between MPTMS and e-GO NSs was synergistically evaluated using Raman and FTIR analyses, which provide complementary and reliable identification of chemical bonding and interfacial interactions. The dispersion behavior and long-term dispersion stability of epoxy/CSB-eGO nanocomposites were assessed by monitoring the distribution of CSB-eGO within the epoxy matrix through photographic documentation and visual observation of phase separation or sedimentation at different time intervals.

2.6. Mechanical and anti-corrosion characterization of epoxy/CSB-eGO nanocomposites

The corrosion resistance of epoxy/CSB-eGO nanocomposite coatings was evaluated using electrochemical impedance spectroscopy (EIS) and Tafel polarization measurements performed on a PalmSens4 electrochemical workstation operated in corrosion analysis mode. A series of epoxy/CSB-eGO nanocomposite coatings with different CSB-eGO loadings (0.10, 0.25, 0.50, 0.75, 1.00, and 1.50 wt%) were prepared to systematically investigate the influence of CSB-eGO content on the corrosion protection performance. Structural steel substrates (SS400 grade) were used as the metallic substrates for coating deposition. The epoxy/CSB-eGO nanocomposite resin was mixed with TETA as the curing agent at a fixed content of 5.0 wt%, and the resulting mixture was applied onto the SS400 steel surface using a doctor blade coating technique with a stainless-steel fixed-gap film applicator set to a gap height of 50 μm. All electrochemical measurements were conducted in accordance with ASTM G59 and ASTM G102 standards at room temperature in a 3.5 wt% NaCl aqueous solution. A conventional three-electrode configuration was employed, consisting of a saturated Ag/AgCl reference electrode, a platinum counter electrode, and the coated SS400 steel as the working electrode. Prior to testing, all electrodes were carefully cleaned to ensure measurement accuracy and reproducibility. For EIS measurements, the frequency range was set from 10^5 to 10^{-2} Hz with a sinusoidal perturbation amplitude of 5 mV. Potentiodynamic polarization tests were carried out at a scan rate of 2 mV s^{-1} over a potential range from −1.0 to +1.0 V, with an exposed working electrode area of 1.0 cm^2.

3. Results and discussion

3.1. Electrochemical formation and characterization of hydrophilic e-GO nanosheets

Fig. 1 presents the structural and surface characterization of electrochemically synthesized graphene oxide (e-GO) NSs. The SEM image (Fig. 1a) reveals a typical sheet-like morphology with pronounced wrinkling and crumpling, indicating effective exfoliation of the parent graphite during the electrochemical process. The thin, loosely stacked, and highly folded nanosheets suggest simultaneous intercalation, oxidation, and delamination of graphite layers under the applied electric field, resulting in e-GO with a substantially developed surface area and abundant edge sites. Such morphological features are characteristic of graphene oxide produced *via* electrochemical routes and are favorable for the formation and exposure of surface functional groups. The TEM image (Fig. 1b) further confirms the nanosheet structure and high degree of exfoliation of e-GO. The presence of semi-transparent regions and limited layer stacking indicates few-layer to near single-layer graphene oxide. The non-uniform contrast observed across the nanosheets reflects spatial variations in oxidation degree, while the irregular edges and defect-rich domains provide direct evidence of disruption of the sp^2 carbon lattice. These defect sites and open edges are known to preferentially host oxygen-containing functional groups, thereby playing a critical role in subsequent covalent surface functionalization. Additional SEM images at wider observation areas (Fig. 1c and d) further demonstrate the uniform exfoliation behavior and effective delamination of the electrochemically synthesized e-GO NSs over large areas. Notably, distinct boundaries of individual e-GO NSs are not clearly observable in the wide-area SEM images. Instead, overlapping and continuous ultrathin e-GO NSs are observed throughout the SEM images, indicating a high degree of electrochemical exfoliation. Furthermore, the absence of obvious thick graphitic platelets or severely restacked aggregates further confirms the effective delamination of graphite during the electrochemical synthesis process. Such highly exfoliated ultrathin nanosheet morphology is highly advantageous for achieving uniform dispersion and efficient surface functionalization in subsequent modification processes. Raman spectroscopy (Fig. 1e) provides quantitative insight into the defect density and structural disorder of e-GO. Two characteristic peaks corresponding to the D band (1335 cm^{-1}) and G band (1600 cm^{-1}) are clearly observed.[36] Notably, the intensity ratio of the D to G bands (I_D/I_G) is calculated to be 1.8, indicating a high density of structural defects induced by electrochemical oxidation.[37] Such a high I_D/I_G ratio reflects substantial disruption of the sp^2-hybridized carbon network and the conversion of sp^2 carbon into sp^3 configurations due to the incorporation of oxygen-containing functional groups. This defect-rich structure is a distinctive feature of electrochemically synthesized GO and is highly advantageous for chemical functionalization, as these defects serve as effective anchoring sites for covalent bonding reactions. In addition, the weakened and broadened 2D band further confirms the loss of long-range π-conjugation and the formation of graphene oxide with a highly oxidized and defective structure. The surface chemical composition of e-GO is further elucidated by FTIR spectroscopy (Fig. 1f). A broad absorption band in the range of 2890–3700 cm^{-1} is assigned to O–H stretching vibrations of hydroxyl and carboxyl groups, indicating a high density of surface hydroxyl functionalities and extensive hydrogen bonding. The distinct peak at ∼1510–1740 cm^{-1} corresponds to C=O stretching vibrations of carbonyl and carboxyl groups.[38] These characteristic FTIR

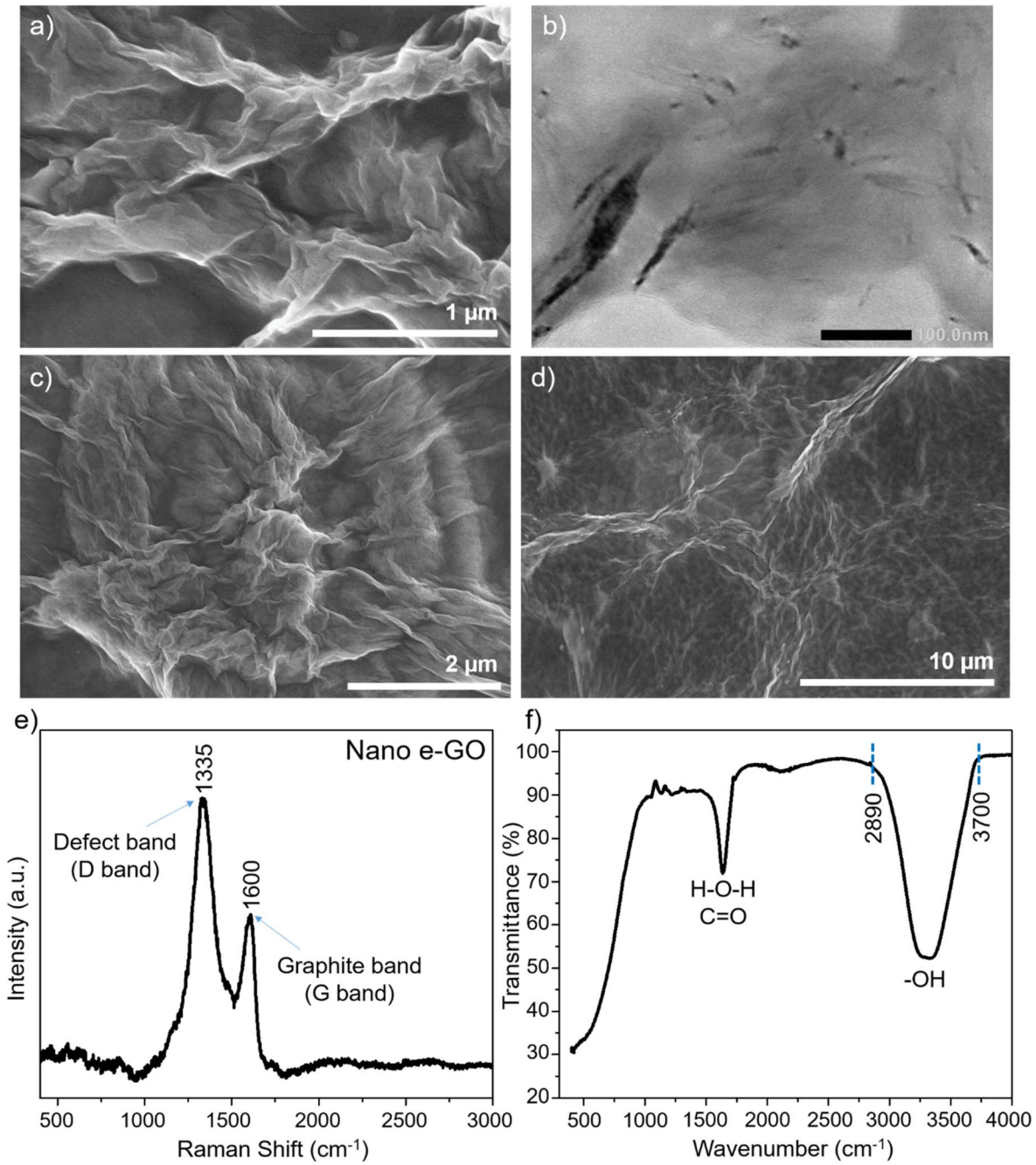

Fig. 1 FE-SEM images at different magnifications (a, c and d), TEM image (b), Raman spectrum (e), and FTIR spectrum (f) of e-GO nanosheets (e-GO NSs).

features confirm the coexistence of multiple oxygen-containing functional groups distributed on both the basal planes and edges of the e-GO nanosheets. Collectively, the SEM and TEM results demonstrate that the electrochemical process successfully produces highly exfoliated graphene oxide nanosheets with large surface area, abundant defects, and open edges, while Raman and FTIR analyses provide compelling evidence for a defect-rich structure ($I_D/I_G = 1.8$) and intrinsically abundant oxygen-containing functional groups. Importantly, these functional groups are generated directly during electrochemical synthesis in an aqueous environment, eliminating the need for additional activation or pretreatment steps prior to surface modification. This combination of morphological characteristics and surface chemistry renders electrochemically synthesized e-GO an ideal platform for subsequent covalent surface functionalization, forming the basis for its effective chemical integration into epoxy matrices.

3.2. Interfacial incompatibility of hydrophilic e-GO with epoxy and covalent silane-bridging strategies

Achieving high-performance polymer nanocomposites, particularly epoxy-based systems, critically depends on the uniform

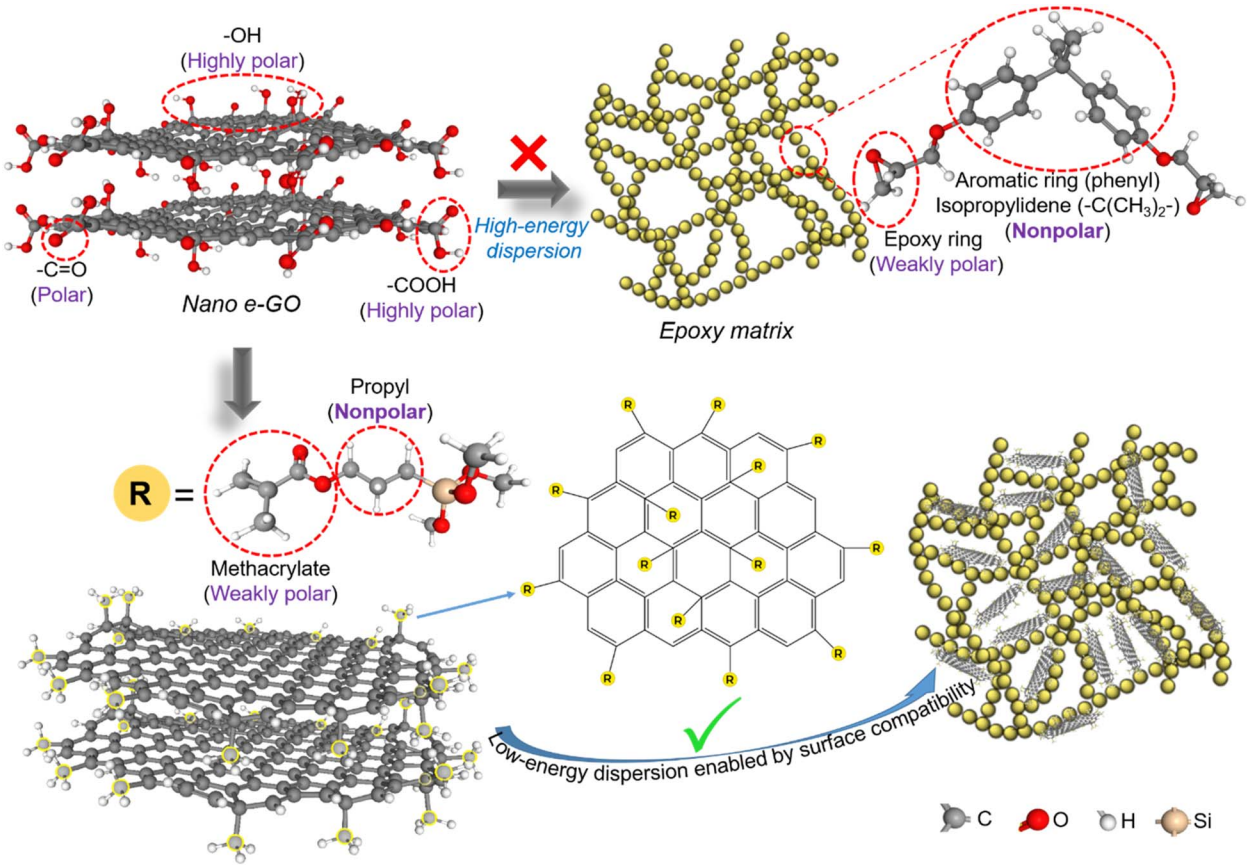

Fig. 2 Schematic illustration of the interfacial incompatibility between hydrophilic e-GO nanosheets and the epoxy matrix, and the silane-bridging strategy to overcome this limitation.

and stable dispersion of nanofillers within the polymer matrix. At a fundamental level, such dispersion is governed by interfacial compatibility between the nanofiller surface and the surrounding polymer chains. However, in many practical systems, the surface chemistry of nanomaterials and polymer matrices is inherently mismatched or even contradictory, leading to severe challenges in dispersion control and long-term stability. As schematically illustrated in Fig. 2, electrochemically exfoliated graphene oxide (e-GO) nanosheets exhibit pronounced interfacial incompatibility with the intrinsically hydrophobic epoxy matrix. This incompatibility originates from a substantial disparity in surface chemistry and polarity between the two phases. Electrochemical e-GO is characterized by a high density of polar oxygen-containing functional groups, including highly polar hydroxyl (–OH) and carboxyl (–COOH) moieties, as well as polar carbonyl (C=O) groups. The abundance of these polar functionalities imparts high surface energy to e-GO and a strong affinity toward polar environments. In contrast, epoxy resins are dominated by molecular motifs with markedly lower polarity, including weakly polar epoxy rings and largely nonpolar aromatic phenyl and isopropylidene (–$C(CH_3)_2$–) segments. This pronounced polarity mismatch severely limits the wettability of epoxy chains on the e-GO surface, forcing the composite system into an energetically unfavorable dispersion state. As a consequence, e-GO nanosheets tend to aggregate through strong intersheet hydrogen bonding and van der Waals interactions among their hydrophilic surfaces, particularly during processing and under prolonged service conditions. Such aggregation not only compromises dispersion uniformity but also introduces interfacial defects, ultimately undermining the mechanical integrity, barrier performance, and long-term reliability of epoxy/e-GO nanocomposites.

Therefore, to fundamentally resolve the issues of dispersion and long-term dispersion stability, addressing interfacial compatibility must be regarded as the core strategic challenge. Among the available approaches, surface modification of the reinforcing nanophase represents the most feasible and effective route, as nanofillers typically constitute only a small fraction of polymer nanocomposites, usually below 5.0 wt%. As discussed above, the surface polarity of nanomaterials can be tailored either through weak physical interactions or through robust chemical bonding. Although surface modification based on weak physical interactions is relatively simple to implement, such interactions are inherently unstable and can be readily disrupted during processing or deteriorate over prolonged service periods. In contrast, the formation of strong chemical bonds to regulate the surface polarity of nanofillers provides a more definitive and durable solution for achieving interfacial compatibility with polymer matrices. However, this approach

imposes a critical requirement on the careful selection of a surface ligand that can simultaneously establish stable covalent bonding with the nanofiller surface and exhibit high chemical compatibility with the polymer network. The choice of an appropriate surface ligand therefore directly determines the effectiveness of surface modification, as well as the dispersion quality and long-term stability of nanofillers within the polymer matrix. As proposed in Fig. 2, a covalent silane-bridging strategy is introduced to deliberately tailor the surface polarity and surface energy of e-GO nanosheets. The selected silane ligand was judiciously designed to fulfill two essential functions: enabling covalent attachment to the e-GO surface and providing optimal compatibility with the epoxy matrix. As illustrated in Fig. 2, the silane molecule possesses an asymmetric structure with two distinct functional domains. The silane head group contains hydrolyzable Si–OR moieties capable of forming covalent bonds with the densely distributed –OH and –COOH groups on the e-GO surface, while the outward-oriented organic segment is specifically designed to interact favorably with the epoxy network. Upon hydrolysis, the silane head group is converted into silanol (Si–OH) groups, which subsequently undergo condensation reactions with surface –OH or –COOH groups on e-GO to form stable Si–O–C and/or Si–O–Si covalent linkages. This process effectively anchors the silane molecules onto the e-GO nanosheets, creating a robust and stable interphase layer. Conversely, the organic segment of the silane comprises propyl groups with near-zero polarity (~0.0) and methacrylate groups with intermediate polarity (1.1–1.4), which were deliberately selected to bridge the polarity gap between e-GO and epoxy. These functional groups exhibit high compatibility with the relatively low-polarity structural motifs of epoxy resins, including epoxy rings (1.0–1.3), aromatic rings, and isopropylidene groups (~0.0), thereby enhancing wettability and interfacial interactions. Based on this interfacial design principle, 3-methacryloxypropyltrimethoxysilane (MPTMS) was selected in this study as a representative silane-bridging agent. MPTMS simultaneously satisfies the requirements for strong covalent bonding with the e-GO surface through its

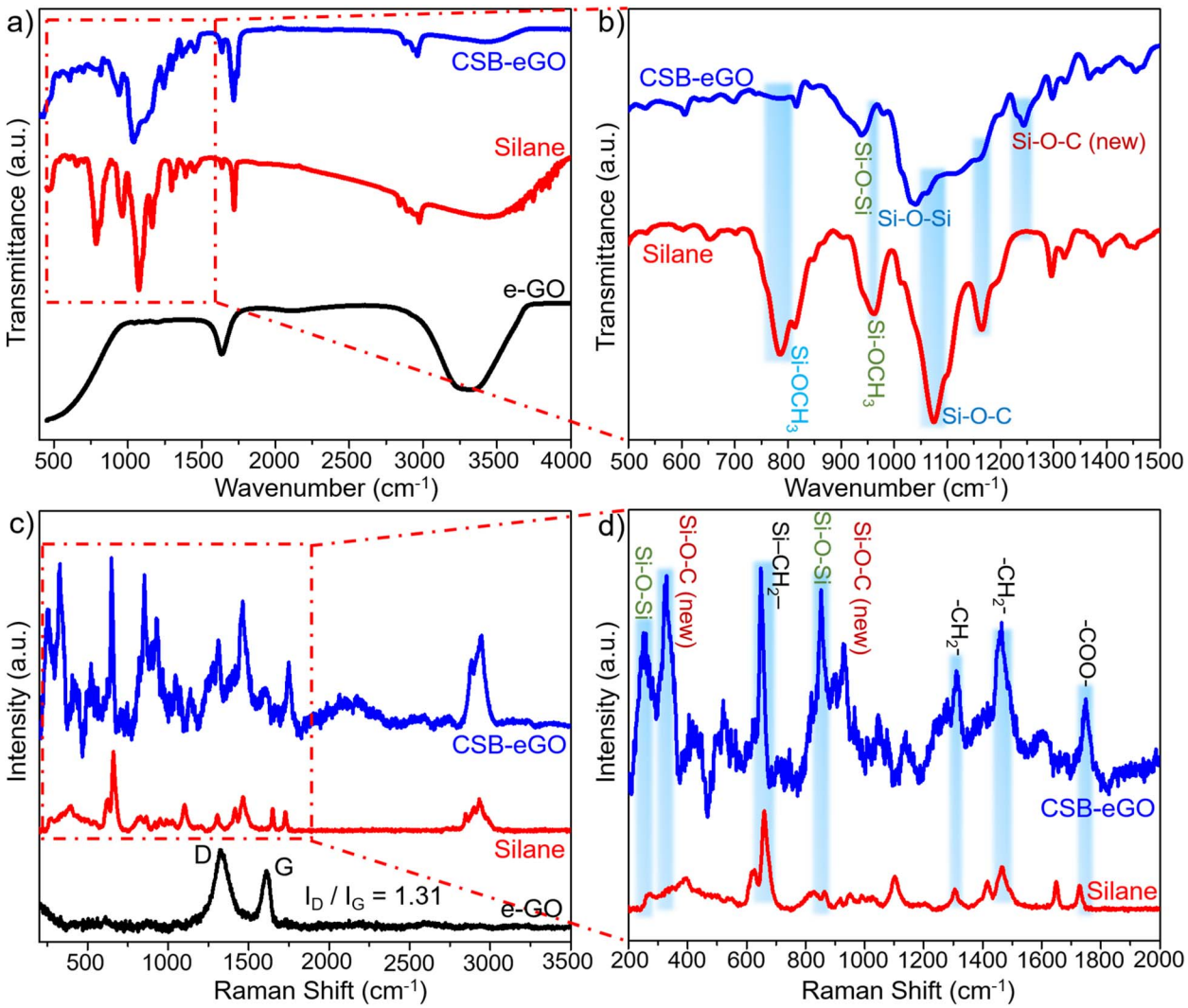

Fig. 3 FTIR spectra (a and b) and Raman spectra (c and d) of e-GO NSs, MPTMS and covalently silane-bridged e-GO nanosheets (CSB-eGO NSs), confirming the successful surface modification of e-GO.

trimethoxysilane head group and optimal chemical compatibility with the epoxy matrix through its propyl spacer and methacrylate functionality. Owing to its bifunctional bridging structure, the silane not only markedly reduces the surface polarity and surface energy of e-GO, but also transforms the nanosheet surface from a hydrophilic to an epoxy-compatible state. This targeted interfacial regulation drives the system toward a lower-energy dispersion state, suppresses re-aggregation, and establishes the foundation for long-term dispersion stability and efficient stress transfer across the nano–polymer interface.

3.3. Formation mechanism, characterization, and long-term dispersion stability of covalently silane-bridged e-GO nanosheets (CSB-eGO NSs) in epoxy resin

The covalent silanization of e-GO nanosheets is described in detail in Section 2.2. As discussed in Section 3.1, FTIR and Raman analyses confirm that pristine e-GO nanosheets are intrinsically hydrophilic, with the coexistence of multiple oxygen-containing functional groups distributed over both the basal planes and edges of the e-GO nanosheets. Fig. 3 presents complementary FTIR and Raman results that collectively verify the successful surface modification of e-GO by MPTMS through the formation of stable covalent bonds. A direct comparison between the FTIR and Raman spectra of pristine MPTMS and those of MPTMS-modified e-GO reveals characteristic spectral changes associated with silanization (Fig. 3a and b). In the FTIR spectrum of pristine MPTMS, the characteristic band at 781 cm^{-1}, corresponding to the Si–O–CH_3 stretching vibration of alkoxy groups, completely disappears after surface treatment, indicating the hydrolysis of methoxy groups into silanol (Si–OH). Concurrently, the band at 1166 cm^{-1}, assigned to the Si–O–C (alkoxy) stretching vibration, exhibits a pronounced decrease in intensity, further confirming the consumption of –OCH_3 groups during hydrolysis. Notably, the characteristic band of MPTMS at 955 cm^{-1} shifts to 933 cm^{-1} in the silanized e-GO sample, reflecting a change in the local chemical environment of the Si atom from an alkoxy configuration to

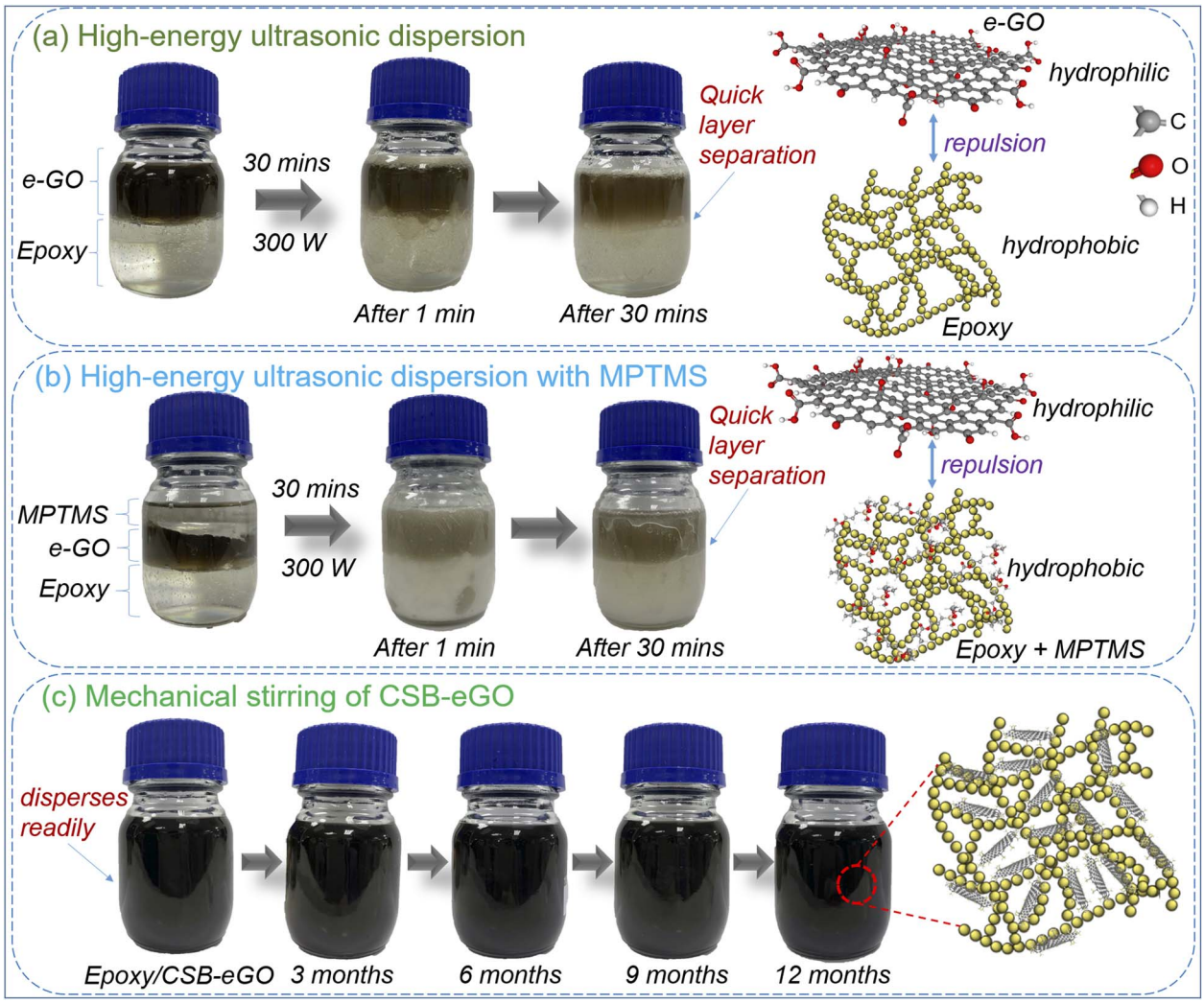

Fig. 4 Comparison of dispersion efficiency and long-term stability of hydrophilic e-GO and covalently silane-bridged e-GO (CSB-eGO) in epoxy resin: (a) dispersion behavior of hydrophilic e-GO in epoxy after ultrasonication; (b) dispersion behavior of e-GO in epoxy in the presence of MPTMS without covalent bonding; (c) homogeneous dispersion and year-long stability of CSB-eGO in epoxy.

a condensed structure or covalent linkage with the e-GO surface (Si–O–Si or Si–O–C). After silanization, a new absorption band emerges at 1036 cm^{-1} in the FTIR spectrum of the modified e-GO, which is attributed to the asymmetric stretching vibration of Si–O–Si bonds, providing direct evidence for the formation of a siloxane network on the nanosheet surface. In addition, a new band at 1242 cm^{-1}, absent in the spectrum of pristine MPTMS, is assigned to Si–O–C vibrations, serving as strong evidence for covalent bonding between silanol groups and surface –OH or –COOH functionalities on e-GO. Further spectral changes in the regions of 3288 cm^{-1} (O–H stretching) and 1641 cm^{-1} (H–O–H bending) indicate a reduction in hydroxyl groups and adsorbed water, consistent with their participation in condensation reactions with silanol groups to form Si–O–C linkages. Importantly, the characteristic bands associated with the methacrylate organic framework, including those at 657 cm^{-1} (Si–C), 1306 and 1465 cm^{-1} (–CH_2– and –CH_3 bending vibrations), and 1729 cm^{-1} (C=O stretching of ester groups), are preserved after silanization, demonstrating that the organic moiety of MPTMS remains intact during the modification process. Raman spectroscopy provides complementary confirmation of successful silanization (Fig. 3c and d). New Raman bands appearing at 250 and 325 cm^{-1}, which are absent in pristine MPTMS, are characteristic of network vibrations of siloxane (Si–O–Si) structures and bending modes of Si–O–C linkages formed on the e-GO surface. Additionally, the emergence of bands at 850 and 930 cm^{-1} further substantiates the presence of Si–O–C and Si–O–Si structures with distinct chemical environments, characteristic of silane condensation and network formation on the carbon framework. The persistence of Raman bands at 1306, 1465, and 1729 cm^{-1} once again confirms the retention of the methacrylate framework of MPTMS. Collectively, the complementary FTIR and Raman analyses unambiguously demonstrate that MPTMS undergoes hydrolysis and is successfully grafted onto the surface of e-GO nanosheets through stable Si–O–C and Si–O–Si covalent bonds, while preserving the methacrylate functionality. This well-defined interfacial architecture provides a favorable chemical foundation for enhanced compatibility with the epoxy matrix.

The FTIR and Raman results confirm the successful surface functionalization of e-GO at the molecular level; the macroscopic consequences of this interfacial regulation are clearly manifested by the distinct dispersion behavior and long-term dispersion stability of e-GO and CSB-eGO in epoxy, as shown in Fig. 4. As shown in Fig. 4a, hydrophilic e-GO was introduced into the epoxy matrix using high-energy ultrasonication (300 W, 30 min). Although ultrasonication can initially disrupt large agglomerates and generate a transiently dispersed state, rapid and pronounced phase separation is observed shortly thereafter. This behavior indicates that the achieved dispersion corresponds to a high-energy, non-equilibrium state maintained primarily by forced mechanical input rather than by stable interfacial interactions. The fundamental origin of this instability lies in the severe polarity mismatch between the e-GO

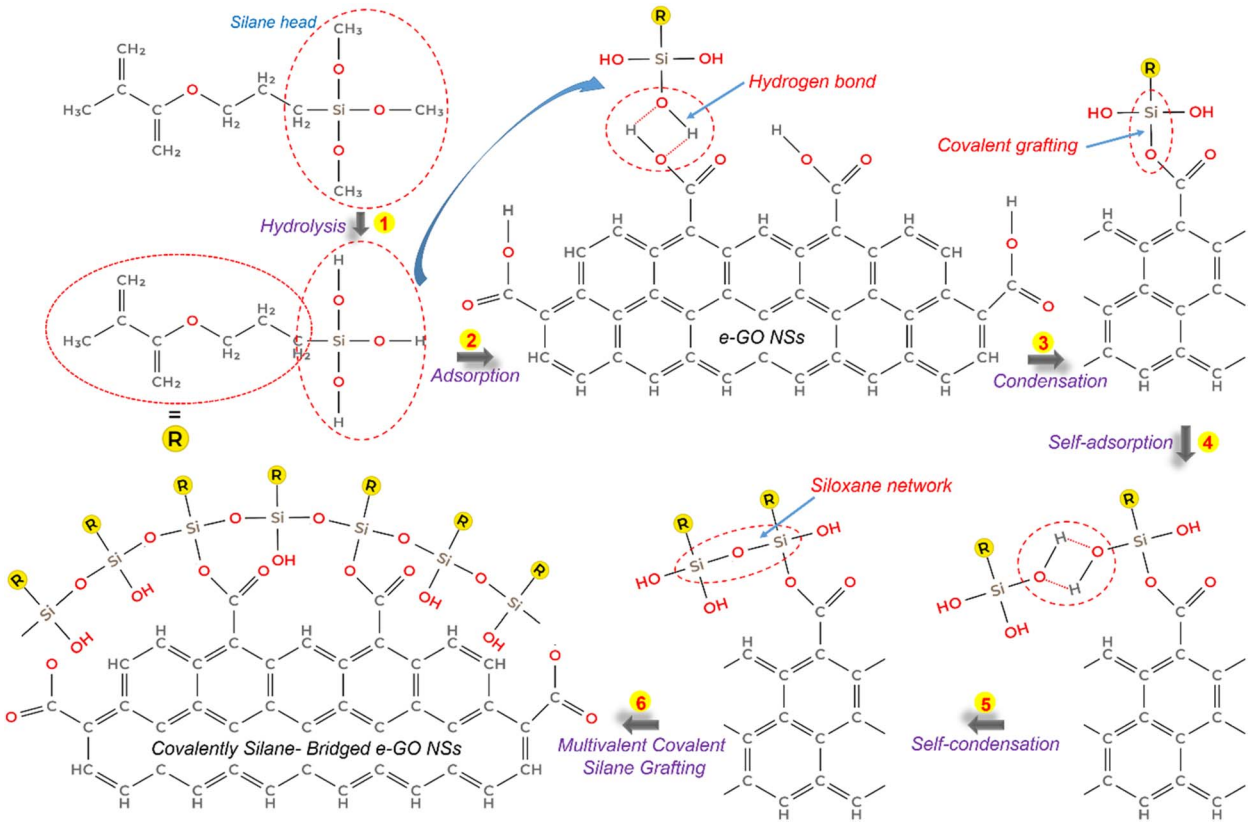

Scheme 2 Schematic illustration of the stepwise formation mechanism of covalently silane-bridged e-GO nanosheets (CSB-eGO NSs), involving silane hydrolysis, interfacial adsorption, condensation, and multivalent covalent grafting.

surface, enriched with –OH and –COOH groups, and the hydrophobic epoxy matrix, which induces strong interfacial repulsion and drives rapid re-aggregation of e-GO nanosheets once ultrasonic agitation ceases. Fig. 4b presents the dispersion behavior of e-GO in epoxy in the presence of MPTMS without covalent bonding. While the addition of MPTMS partially improves the wettability of the e-GO surface and moderately retards phase separation compared to Fig. 4a, the system still exhibits rapid sedimentation and poor long-term stability. This observation demonstrates that weak physical interactions or non-covalent adsorption of MPTMS are insufficient to fundamentally overcome the polarity and surface energy mismatch between e-GO and epoxy, particularly in the absence of continuous mechanical agitation. In sharp contrast, Fig. 4c reveals a fundamentally different dispersion behavior for CSB-eGO in epoxy. Even under simple mechanical stirring, CSB-eGO readily disperses to form a homogeneous system, with no observable phase separation or sedimentation after prolonged storage for up to 12 months. This exceptional long-term stability indicates that the surface of CSB-eGO has been effectively regulated from both chemical and interfacial compatibility perspectives, enabling the system to reach a low-energy and intrinsically stable dispersion state. The presence of covalent silane bridges markedly reduces the surface polarity and surface energy of e-GO while simultaneously imparting chemical compatibility with the epoxy network, thereby eliminating interfacial repulsion and suppressing nanosheet re-aggregation. Collectively, these macroscopic observations unequivocally demonstrate the essential role of covalent silane bridging in governing the dispersion behavior of e-GO in epoxy. More importantly, they highlight that long-term dispersion stability cannot be achieved solely through mechanical dispersion or temporary physical modification. Instead, directed interfacial regulation at the molecular level is a prerequisite for fully exploiting the reinforcing potential of e-GO in epoxy composites designed for durable, real-world applications.

Based on the FTIR and Raman evidence confirming the formation of covalent Si–O–C and Si–O–Si linkages on the e-GO surface, Scheme 2 proposes a detailed mechanism for the silanization process and the development of the silane interphase on e-GO nanosheets. This process does not proceed *via* a single reaction step; rather, it involves a sequence of synergistic and consecutive reactions, including silane hydrolysis, interfacial adsorption, condensation, and multivalent covalent grafting. Following hydrolysis of the alkoxy groups of MPTMS into silanol species, the silane molecules are initially anchored onto the e-GO surface through physical adsorption and hydrogen bonding with the densely distributed –OH and –COOH groups

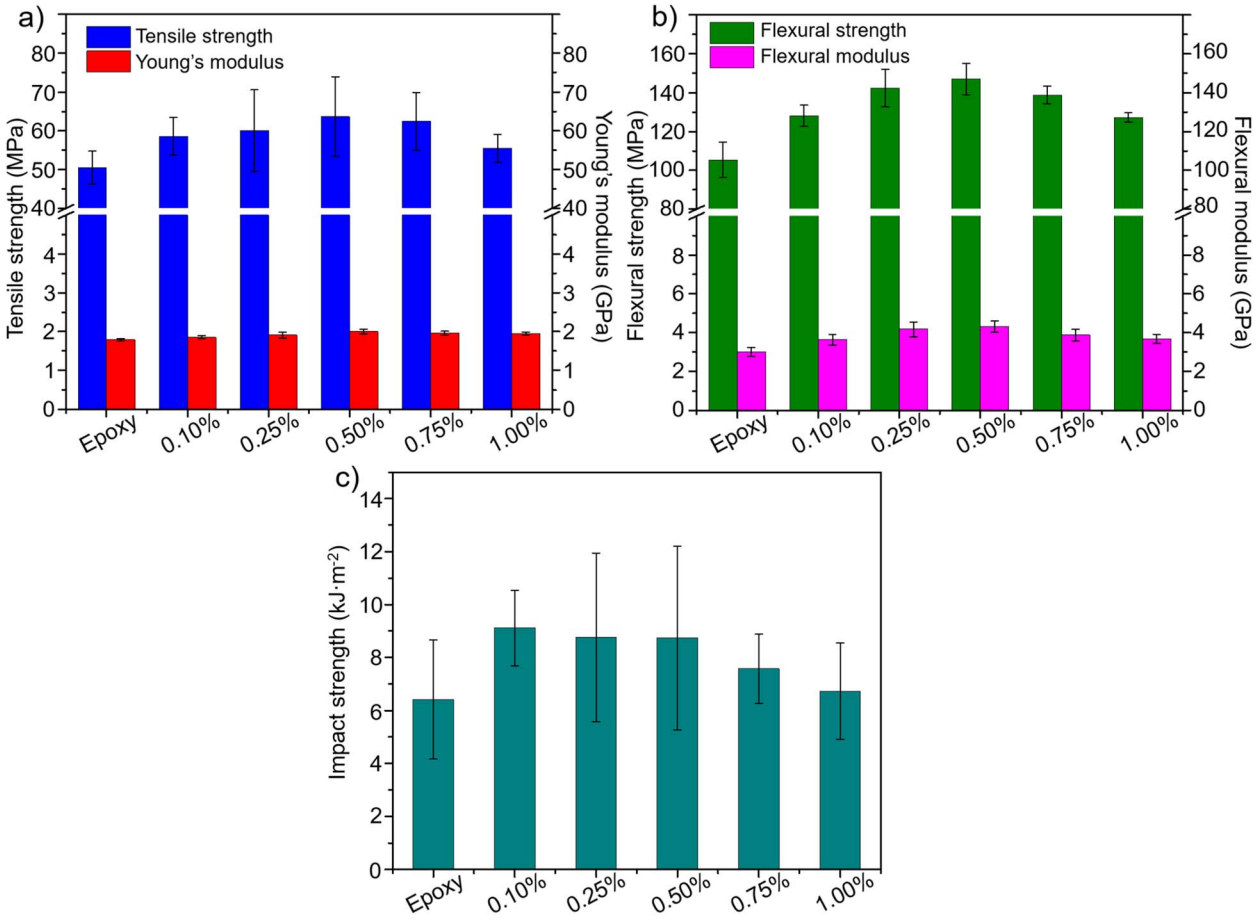

Fig. 5 Mechanical properties of epoxy and epoxy/CSB-eGO nanocomposites: (a) tensile strength and Young's modulus, (b) flexural strength and flexural modulus, and (c) impact strength.

located on both the basal planes and edges of the e-GO nanosheets.[39] This interfacial adsorption stage facilitates the oriented arrangement of silane molecules at the interface, thereby increasing the effective contact probability between –SiOH groups and reactive oxygen-containing sites on e-GO. Upon elevating the reaction temperature, condensation reactions are activated, leading to the formation of covalent Si–O–C linkages between silane molecules and the e-GO surface, while simultaneous self-condensation among silanol groups generates a crosslinked Si–O–Si network. Owing to the presence of three hydrolyzable –SiOH groups per MPTMS molecule, each silane unit can participate in multiple condensation reactions, giving rise to a multivalent covalent grafting mechanism and the progressive growth of a continuous polysiloxane network that envelops the e-GO nanosheets. This silane network not only robustly anchors the silane molecules onto the e-GO surface, but also functions as a hybrid inorganic–organic interphase layer, markedly reducing the surface energy and effectively regulating the surface polarity of e-GO. Importantly, the methacryloxypropyl organic tail of MPTMS is preserved and oriented outward after modification, imparting a hydrophobic surface character with high chemical compatibility toward the epoxy network. Consequently, the silane-bridging mechanism illustrated in Scheme 2 not only elucidates the molecular-level chemical transformations induced by silanization, but also reveals the fundamental origin of the altered dispersion behavior of e-GO in epoxy. The formation of a robust, covalently bonded silane network enables the system to transition from a mechanically dispersed and poorly compatible state to a highly stable and well-dispersed interfacial state. This interfacial architecture therefore underpins the uniform dispersion and long-term stability of CSB-eGO in epoxy resin, as clearly manifested by the macroscopic observations in Fig. 4.

3.4. Mechanical reinforcement: tensile, flexural, and impact properties

Fig. 5 summarizes the influence of CSB-eGO loading on the key mechanical properties of the epoxy system, including tensile strength and Young's modulus (Fig. 5a), flexural strength and flexural modulus (Fig. 5b), as well as impact strength (Fig. 5c). The results demonstrate that reinforcing epoxy with CSB-eGO leads to simultaneous and pronounced improvements in both strength and stiffness at low nanofiller contents, reflecting the high reinforcing efficiency of e-GO nanosheets when dispersion state and interfacial interactions are effectively controlled. Compared with neat epoxy (tensile strength of 50.5 MPa and Young's modulus of ~1.79 GPa), the incorporation of CSB-eGO at loadings of 0.10–0.50 wt% results in a marked increase in tensile strength, reaching a maximum value of 63.6 MPa at 0.50 wt% CSB-eGO, corresponding to an enhancement of approximately 26%. Concurrently, Young's modulus increases from ~1.79 GPa to nearly 2.00 GPa, indicating a substantial increase in material stiffness (Fig. 5a). A similar trend is observed for flexural properties. The flexural strength increases from approximately 105 MPa for neat epoxy to nearly 150 MPa at 0.50 wt% CSB-eGO, representing an improvement of about 43%, while the flexural modulus rises from ~3.0 GPa to approximately 4.3 GPa (Fig. 5b). The concurrent enhancement of both strength and modulus indicates that CSB-eGO functions not merely as a high-modulus rigid filler, but also actively

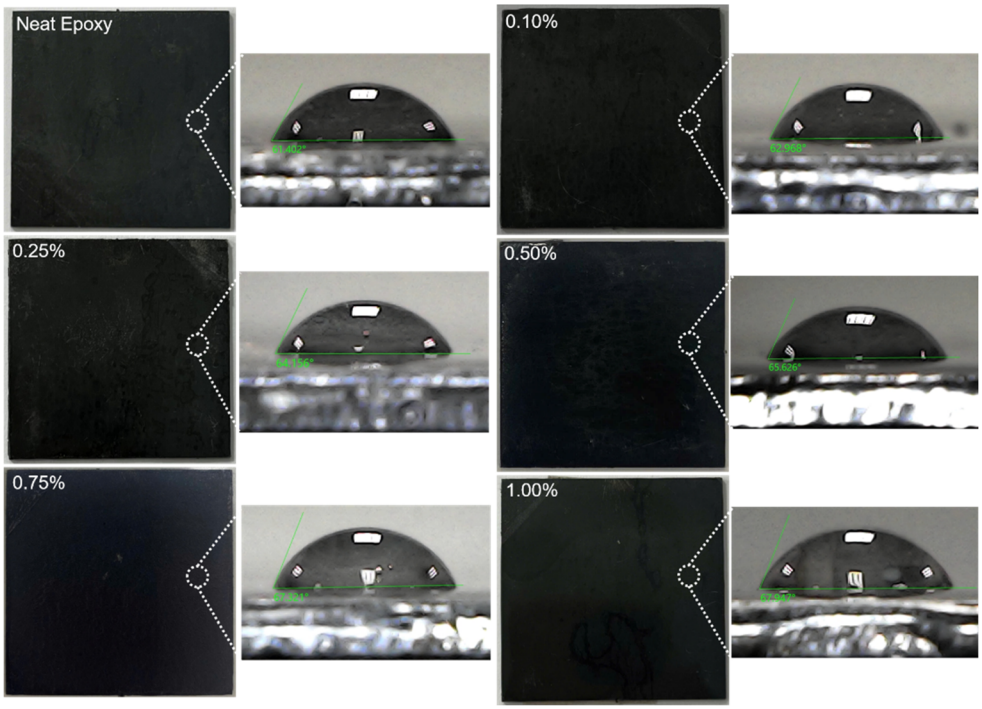

Fig. 6 Optical photographs and water contact angle measurements of neat epoxy and epoxy/CSB-eGO nanocomposite coatings with different CSB-eGO loadings after curing.

participates in efficient stress transfer throughout the composite. The pronounced mechanical reinforcement can be attributed to the synergistic contribution of three key factors. First, CSB-eGO is uniformly and stably dispersed within the epoxy matrix, as evidenced in Fig. 4, effectively eliminating stress concentration sites commonly observed in conventional epoxy/GO systems. Second, covalent silane bridges establish a robust interphase between e-GO nanosheets and the epoxy network, enabling efficient load transfer from the polymer matrix to the nanofiller rather than stress dissipation at weak interfaces. Third, the high aspect ratio and two-dimensional morphology of e-GO allow the exceptional intrinsic modulus of graphene to be efficiently exploited even at very low filler loadings. When the CSB-eGO content exceeds the optimal level ($\geq$0.75 wt%), both tensile and flexural properties exhibit a slight decline. This behavior can be attributed to increased nano–nano interactions and the reduced ability of the epoxy matrix to fully wet the nanofiller surface at higher loadings, leading to suboptimal stress transfer efficiency.

The intrinsically low impact strength is one of the most critical and long-standing limitations of epoxy resins, arising from their tightly crosslinked network structure, high crosslink density, and severely restricted plastic deformation capability.[40,41] Consequently, any reinforcement strategy that can substantially enhance impact resistance without compromising other mechanical properties is of particular significance for both structural and protective coating applications. In this context, the impact strength results presented in Fig. 5c clearly demonstrate the outstanding toughening efficiency of CSB-eGO, especially at ultralow filler loadings. Specifically, the incorporation of only 0.10 wt% CSB-eGO increases the impact strength of epoxy from approximately 6.42 kJ m^{-2} to 8.74 kJ m^{-2}, corresponding to an enhancement of about 36%. Such a pronounced improvement is remarkable for an epoxy system that does not rely on conventional toughening agents such as liquid rubbers or thermoplastic modifiers, and compares favorably with many reported graphene- or carbon nanotube-reinforced epoxy systems, where significant toughening often requires higher filler loadings and is frequently accompanied by a loss in stiffness. Notably, the maximum toughening effect is achieved at the lowest CSB-eGO loading (0.10 wt%), indicating that the dominant toughening mechanism in this system does not originate from a filler crowding effect, but rather from a finely tuned nano–polymer interfacial architecture. At low loadings, multiple energy-dissipation mechanisms operate synergistically and with high efficiency. First, uniformly dispersed CSB-eGO nanosheets, robustly anchored within the epoxy network *via* covalent silane bridges, act as effective nanoscale obstacles that deflect and elongate crack propagation paths. This crack deflection significantly increases the fracture surface area and the energy required for crack advancement under impact loading. Second, the strong yet compliant nano–polymer interphase enables controlled interfacial sliding and localized plastic deformation of the epoxy matrix surrounding the nanosheets, rather than catastrophic brittle fracture as observed in neat epoxy. Third, at ultralow loadings, CSB-eGO does not excessively increase the global stiffness of the system, thereby preserving sufficient matrix deformability necessary for effective impact energy absorption. When the CSB-eGO content exceeds 0.25 wt%, the impact strength no longer improves and instead exhibits a tendency toward saturation followed by gradual decline. This behavior reflects a progressive shift from a toughening regime dominated by energy dissipation to a reinforcement regime governed primarily by stiffness enhancement. At higher filler contents, the increased rigidity and nanofiller density constrain localized matrix deformation and reduce the effectiveness of energy-dissipating mechanisms, leading to diminished impact resistance. Such a trend is consistent with the well-known trade-off between stiffness and toughness in nanofiller-reinforced polymer systems and further underscores the importance of optimizing CSB-eGO loading. Overall, the impact strength results demonstrate that the covalent silane-bridging strategy is not merely effective in enhancing stiffness and strength, but is particularly powerful in overcoming the intrinsic brittleness of epoxy resins. Achieving the highest impact toughness at an ultralow loading of only 0.10 wt% CSB-eGO highlights the exceptional efficiency and material economy of this toughening approach, while maintaining balanced mechanical performance, thereby offering strong potential for epoxy systems requiring high impact resistance and long-term durability.

3.5. Superior anti-corrosive effectiveness and underlying mechanism of epoxy/CSB-eGO nanocomposites

First, the optical appearance after curing and the water contact angle behavior of neat epoxy and epoxy/CSB-eGO nanocomposite coatings with different CSB-eGO loadings were investigated to preliminarily evaluate the coating uniformity, surface wettability, and macroscopic compatibility of CSB-eGO within the epoxy matrix. As shown in Fig. 6, all coatings exhibit relatively smooth, continuous, and defect-free surfaces without obvious macroscopic aggregation or phase separation, indicating good processability and favorable dispersion compatibility of CSB-eGO within the epoxy matrix. In particular, the epoxy/CSB-eGO coatings exhibit visually uniform coating surfaces after curing, further suggesting the formation of homogeneous and compact nanocomposite coatings. The neat epoxy coating exhibits a water contact angle of approximately 61.4°, which is consistent with the typical wettability behavior of commercial epoxy coatings.[42] After incorporation of CSB-eGO nanosheets, the water contact angle does not change significantly and remains within a similar range, although a slight increasing tendency can be observed with increasing CSB-eGO loading. These results indicate that the incorporation of CSB-eGO nanosheets does not adversely affect the intrinsic surface wettability behavior of the epoxy coating system. More importantly, the visually homogeneous coating morphology together with the maintained surface wettability behavior suggests that the incorporation of CSB-eGO does not introduce significant macroscopic defects or phase separation within the coating structure.

The corrosion protection performance of epoxy coatings is fundamentally governed by the coating compactness and its

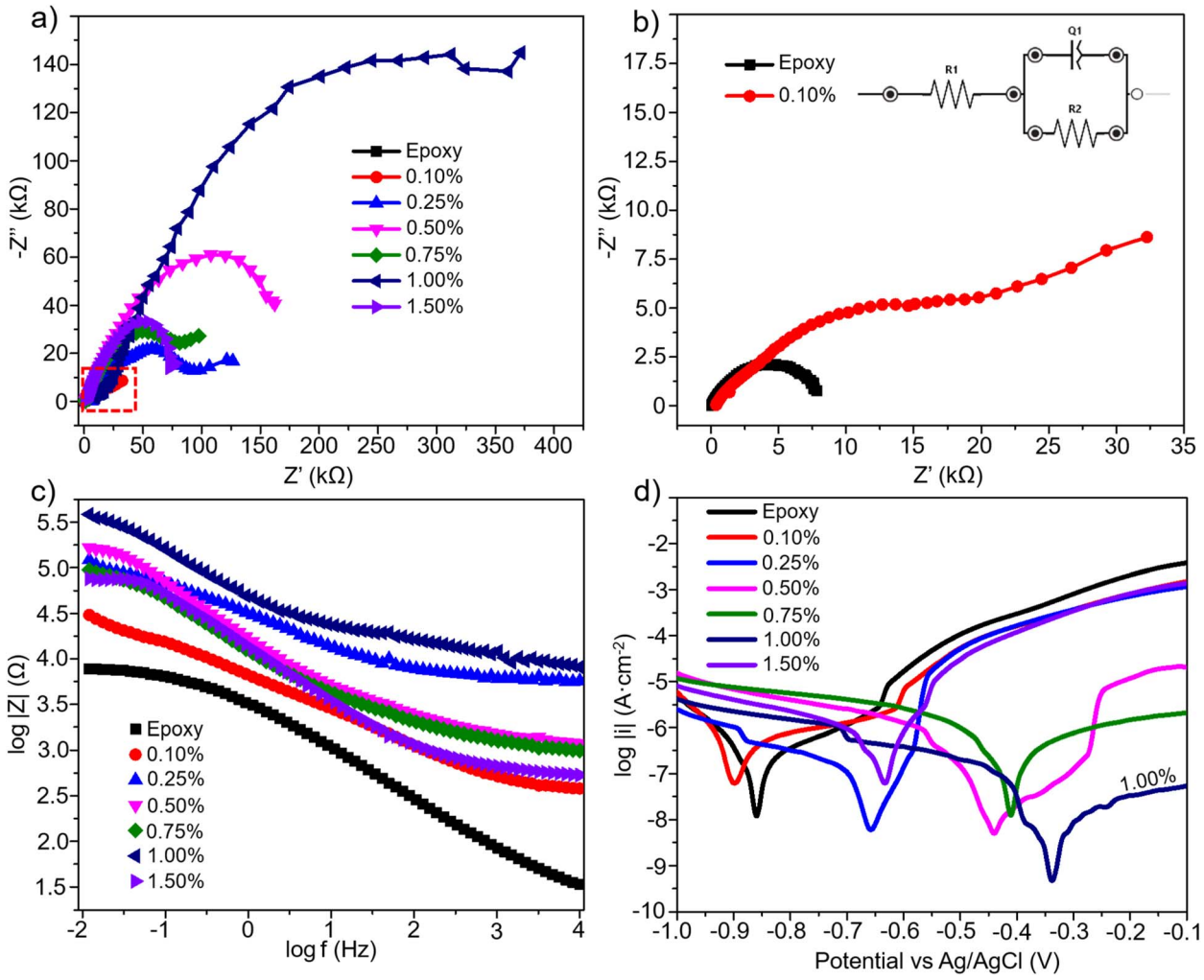

Fig. 7 Electrochemical corrosion behavior of epoxy and epoxy/CSB-eGO nanocomposite coatings with different CSB-eGO loadings measured in 3.5 wt% NaCl solution: (a) Nyquist plots of neat epoxy and epoxy/CSB-eGO coatings with CSB-eGO contents ranging from 0.10 to 1.50 wt%; (b) comparison of Nyquist plots for neat epoxy and epoxy/CSB-eGO containing 0.10 wt% CSB-eGO; (c) Bode magnitude plots of neat epoxy and epoxy/CSB-eGO coatings with CSB-eGO contents ranging from 0.10 to 1.50 wt%; and (d) Tafel polarization curves of neat epoxy and epoxy/CSB-eGO coatings with CSB-eGO contents ranging from 0.10 to 1.50 wt%.

ability to sustain electrical resistance against the ingress of water, oxygen, and aggressive Cl^- ions under corrosive environments. In this context, the pore resistance of the coating (R_{pore}) is widely regarded as the dominant parameter, as it directly reflects moisture permeability and the structural integrity of the coating over time.[43] The electrochemical results presented in Fig. 7 and 8 demonstrate that the incorporation of CSB-eGO into the epoxy matrix leads to a pronounced and durable enhancement in corrosion resistance, while simultaneously elucidating an interphase-controlled protection mechanism.

The Nyquist plots shown in Fig. 7a and b reveal that neat epoxy exhibits only a small capacitive semicircle, indicative of limited resistance to ionic transport through the coating. EIS fitting analysis for the unimmersed neat epoxy coating yields an R_{pore} value of approximately 8.49×10^3 Ω, suggesting a relatively porous coating structure that is susceptible to moisture penetration even at the initial stage. In sharp contrast, the introduction of CSB-eGO results in a systematic and substantial increase in R_{pore} with increasing nanofiller content. Specifically, at 0.10 wt% CSB-eGO, R_{pore} increases to 3.44×10^4 Ω, approximately four times higher than that of neat epoxy. At 0.25 wt%, R_{pore} further rises to 9.73×10^4 Ω, representing an increase of more than one order of magnitude, while the highest R_{pore} value of 2.46×10^5 Ω is achieved at 1.00 wt% CSB-eGO, nearly 30 times greater than that of neat epoxy. This pronounced increase in R_{pore} reflects the formation of a significantly more compact coating architecture, in which the diffusion pathways for water and corrosive ions are effectively narrowed and tortuosity is markedly increased. This trend is further corroborated by the Bode magnitude $|Z|$ plots shown in Fig. 7c. Neat epoxy exhibits the lowest impedance modulus at low frequencies, together with a rapid decline with decreasing frequency, indicative of poor barrier performance and facile electrolyte penetration. In contrast, epoxy/CSB-eGO coatings display substantially higher $|Z|$ values in the low-frequency region, which increase

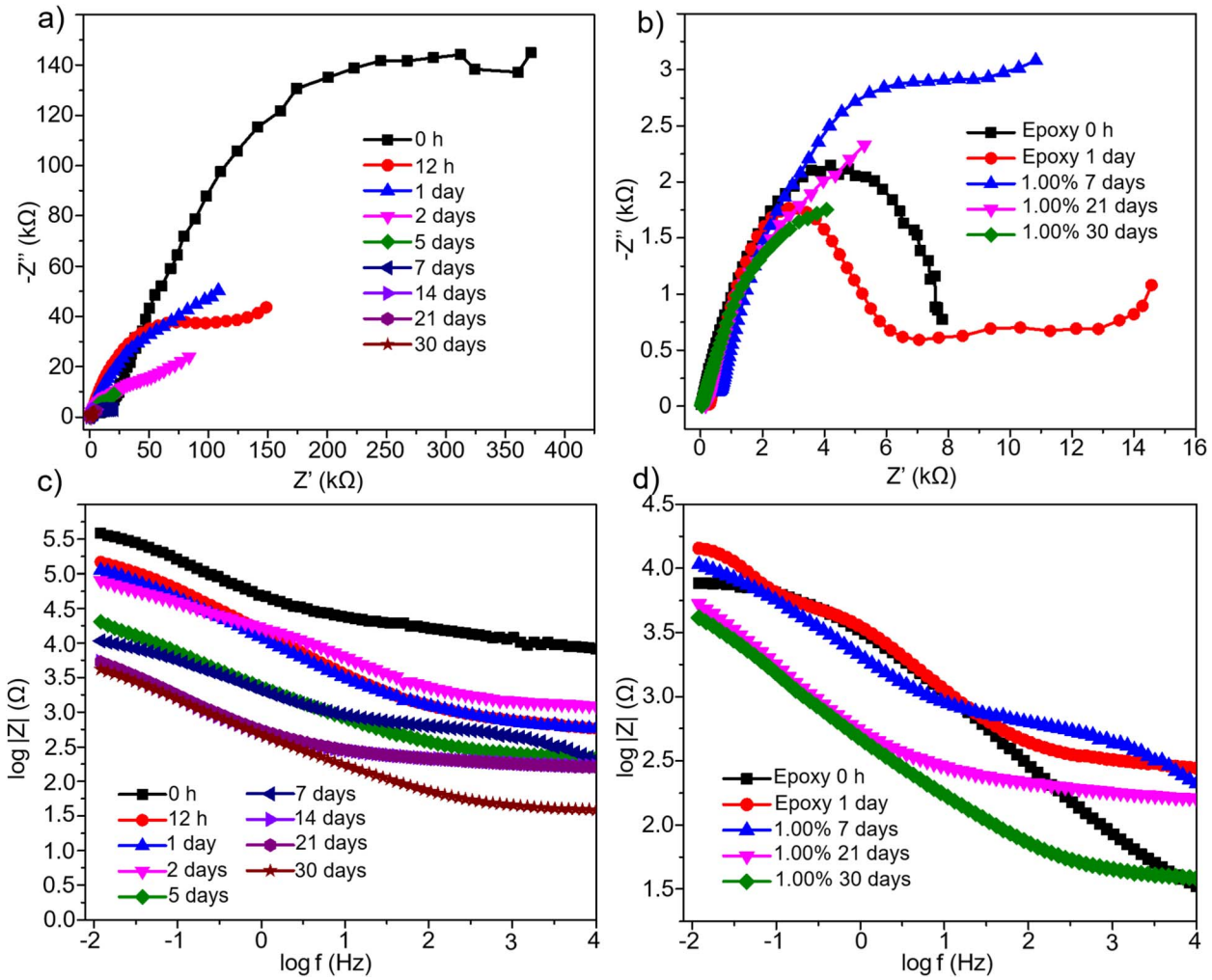

Fig. 8 Time-dependent corrosion protection performance of epoxy/CSB-eGO coatings with a CSB-eGO loading of 1.00 wt% during immersion in 3.5 wt% NaCl solution: (a) Nyquist plots of epoxy/CSB-eGO (1.00 wt%) coatings at different immersion times; (b) comparison of Nyquist plots of epoxy/CSB-eGO (1.00 wt%) after 7, 21, and 30 days of salt immersion with neat epoxy coatings before immersion and after 1 day of immersion; (c) Bode magnitude plots of epoxy/CSB-eGO (1.00 wt%) coatings at different immersion times; and (d) comparison of Bode magnitude plots of epoxy/CSB-eGO (1.00 wt%) after 7, 21, and 30 days of salt immersion with those of neat epoxy coatings before immersion and after 1 day of immersion.

progressively with CSB-eGO loading, reflecting an enhanced resistance to corrosive species ingress. Notably, at CSB-eGO contents of 0.50–1.00 wt%, the sustained high $|Z|$ values in the low-frequency domain approach the behavior of an ideal dielectric coating, characterized by minimal defects and superior barrier integrity. The Tafel polarization curves presented in Fig. 7d provide complementary evidence for the enhanced corrosion protection imparted by CSB-eGO. Compared with neat epoxy, epoxy/CSB-eGO coatings exhibit significantly lower corrosion current densities and a shift of the corrosion potential toward more noble values. The pronounced reduction in corrosion current density indicates an effective suppression of corrosion kinetics, which is fully consistent with the increased R_{pore} values and elevated low-frequency impedance obtained from EIS measurements. These results collectively confirm that epoxy/CSB-eGO coatings not only impede the diffusion of corrosive species, but also retard electrochemical reactions occurring at the metal/coating interface.

The superior corrosion protection performance of epoxy/CSB-eGO is not limited to the initial exposure stage but is effectively maintained during prolonged immersion in 3.5 wt% NaCl solution, as shown in Fig. 8. For neat epoxy coatings, R_{pore} decreases rapidly upon immersion, dropping to approximately 3.18×10^3 Ω after 1 day (Fig. 8b), indicating severe moisture ingress and a pronounced loss of barrier integrity. In sharp contrast, the epoxy/CSB-eGO coating containing 1.00 wt% CSB-eGO retains an R_{pore} value of approximately 1.25×10^4 Ω after 7 days of immersion, which is nearly four times higher than that of immersed neat epoxy and remains even higher than the initial R_{pore} of neat epoxy prior to immersion (Fig. 8a and b). This sustained pore resistance clearly demonstrates the enhanced durability of the barrier structure introduced by CSB-eGO. To further evaluate the long-term corrosion resistance

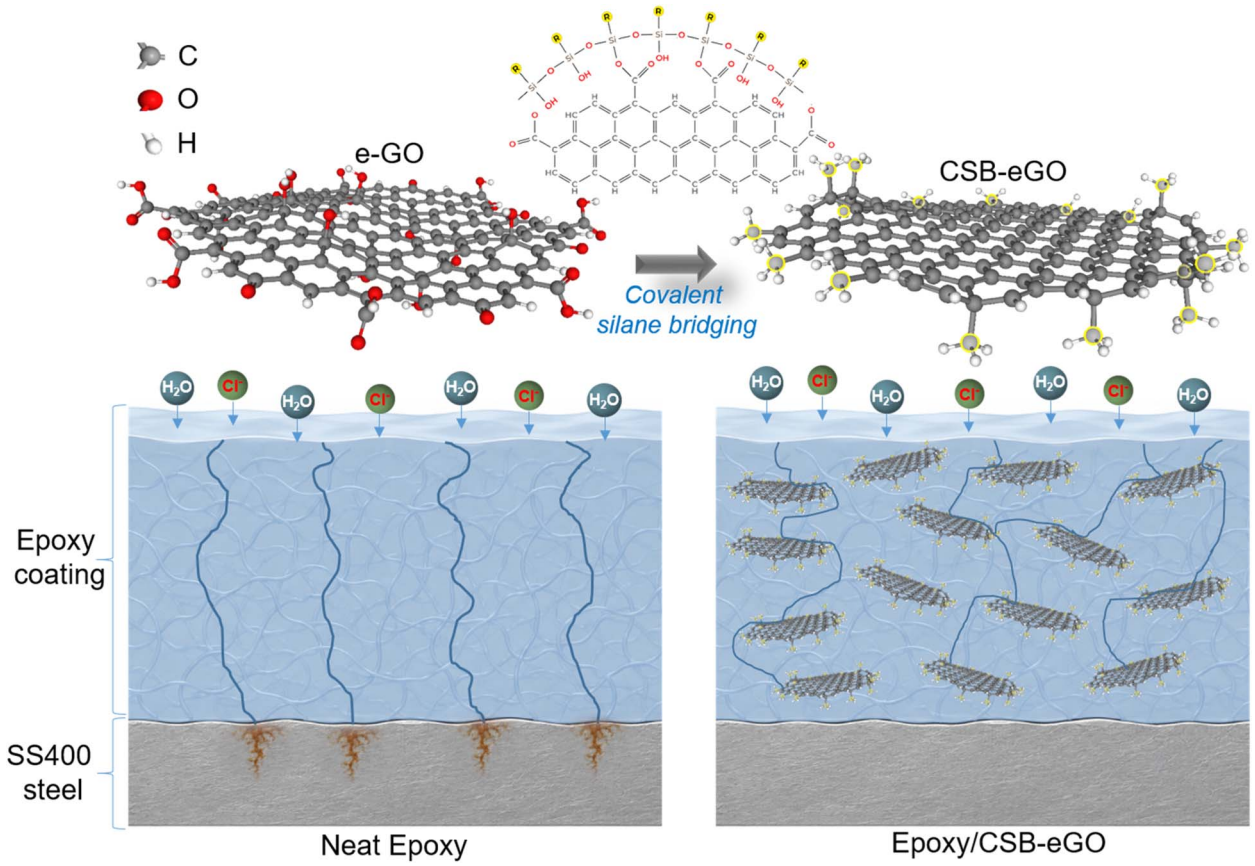

Scheme 3 Schematic illustration of the interphase-controlled corrosion protection mechanism of epoxy/CSB-eGO nanocomposite coatings, compared to neat epoxy coatings.

behavior, extended immersion EIS measurements up to 30 days were additionally performed for the epoxy/CSB-eGO coating. The results reveal that the coating still maintains relatively high pore resistance values of approximately 1.03×10^4 Ω after 14 days of immersion, 9.06×10^3 Ω after 21 days, and 8.10×10^3 Ω after 30 days. Notably, even after 30 days of continuous immersion in 3.5 wt% NaCl solution, the R_{pore} value of the epoxy/CSB-eGO coating remains significantly higher than that of neat epoxy after only 1 day of immersion and is still comparable to the initial R_{pore} of neat epoxy before immersion. These results clearly demonstrate the remarkable long-term barrier durability and corrosion resistance stability imparted by the CSB-eGO nanosheets. This prolonged corrosion resistance behavior is further corroborated by the Bode magnitude plots shown in Fig. 8c and d. While the low-frequency impedance modulus $|Z|$ of neat epoxy decreases sharply with increasing immersion time, reflecting rapid degradation of the coating barrier, the epoxy/CSB-eGO coating exhibits a significantly slower decline and maintains relatively high $|Z|$ values even after 14, 21, and 30 days of immersion. Such behavior indicates that the epoxy/CSB-eGO coating possesses a durable and resilient barrier architecture capable of effectively retarding electrolyte penetration and slowing the progressive loss of coating resistance in corrosive environments.

The above electrochemical results indicate that the corrosion protection mechanism of epoxy/CSB-eGO coatings cannot be attributed solely to the conventional geometric barrier effect of graphene oxide nanosheets. Instead, the protective efficiency is fundamentally governed by nanoscale interfacial regulation enabled by covalent silane bridging. CSB-eGO nanosheets are robustly anchored within the epoxy network, forming a dense and well-integrated interphase that eliminates the interfacial microvoids commonly associated with poorly dispersed fillers. Meanwhile, the silane network grafted onto the e-GO surface significantly reduces its affinity toward water, effectively suppressing the "moisture-trapping" behavior that typically compromises hydrophilic GO in conventional epoxy/GO systems. In addition, the concurrent enhancement of mechanical properties – particularly the pronounced improvement in impact strength discussed in Section 3.4 – plays a critical auxiliary role in corrosion protection. The improved resistance to impact and mechanical deformation mitigates the initiation and propagation of microcracks within the coating under mechanical and environmental stresses. The reduced density of microcracks directly limits the formation of fast diffusion pathways for water and Cl^- ions, thereby contributing to the sustained retention of high R_{pore} and low-frequency impedance $|Z|$ values over extended immersion periods. Taken together, the quantitative EIS fitting results, Bode impedance analysis, and

Tafel polarization measurements consistently demonstrate that epoxy/CSB-eGO coatings exhibit superior and long-term corrosion resistance compared to neat epoxy. The covalent silane-bridging strategy not only enhances the initial pore resistance of the coating but also markedly retards its degradation under prolonged corrosive exposure. These findings confirm that the corrosion protection performance of epoxy/CSB-eGO originates from an interphase-controlled corrosion protection mechanism, in which stable nanofiller dispersion, interphase densification, and mechanically reinforced coating integrity synergistically determine the long-term protective lifetime – surpassing the limitations of traditional barrier mechanisms based solely on geometric tortuosity. The proposed corrosion protection mechanism of the epoxy/CSB-eGO coating system is schematically illustrated in Scheme 3. In conventional neat epoxy coatings, the absence of nanoscale interfacial regulation facilitates the formation of continuous leakage pathways for water and chloride ions, enabling rapid electrolyte penetration toward the coating/steel interface and accelerating localized corrosion initiation. In contrast, covalent silane bridging transforms hydrophilic e-GO into a low-polarity and epoxy-compatible nanofiller, enabling uniform nanosheet dispersion and the formation of a dense interphase within the epoxy matrix. The well-integrated CSB-eGO nanosheets not only generate highly tortuous diffusion pathways that retard water and ion transport, but also reinforce the structural integrity of the coating and suppress the formation of defect-assisted permeation channels. As a result, the epoxy/CSB-eGO coating exhibits significantly enhanced barrier durability and long-term corrosion protection performance.

4. Conclusion

This work presents a covalent silane-bridging strategy to overcome the intrinsic interfacial incompatibility between hydrophilic electrochemically exfoliated graphene oxide (e-GO) and epoxy resin. Through rational molecular design of the silane coupling agent, the surface polarity and interfacial energy of e-GO were precisely tuned *via* multivalent covalent bonding, yielding covalently silane-bridged e-GO nanosheets (CSB-eGO) with excellent compatibility toward the epoxy matrix. Spectroscopic analyses confirmed the formation of stable Si–O–C and Si–O–Si linkages while preserving the organic functionality essential for epoxy interaction. As a result, CSB-eGO achieved highly stable long-term dispersion in epoxy, effectively suppressing nano-agglomeration and interfacial defects that typically limit epoxy/GO systems. Importantly, this interphase-engineered architecture enables long-term dispersion stability at the year-scale, meeting a critical requirement for industrial coating applications. Enabled by a dense and well-integrated interphase, epoxy/CSB-eGO nanocomposites exhibited balanced enhancement of tensile, flexural, and impact properties at ultralow filler loadings. Electrochemical investigations further revealed a pronounced and durable increase in pore resistance, together with elevated low-frequency impedance and suppressed corrosion currents, demonstrating superior and long-lasting corrosion protection under corrosive environments. Notably, the silane-bridging approach relies on a simple, scalable, and solvent-compatible processing route, making it readily adaptable to industrial epoxy formulation and coating processes. By simultaneously addressing dispersion stability, interfacial integrity, mechanical robustness, and corrosion resistance, this work advances epoxy nanocomposites closer to practical, long-term engineering applications.

Author contributions

A.-T. Pham: conceptualization, methodology, supervision, formal analysis; writing – review and editing; Q.-D. Mai: conceptualization, methodology, investigation, formal analysis, project administration; writing – original draft, writing – review and editing; N. T. Loan: validation, investigation, data curation, writing – original draft; N. T. Huy: validation, investigation, data curation; N. T. P. Anh: validation, investigation, data curation; P. C. Thanh: validation, investigation; N. T. Trang: validation, investigation; L. M. Quang: validation, investigation; N. V. Quyet: validation, investigation; T. N. Bach: validation, investigation; A.-T. Le: conceptualization, methodology, supervision, writing – review and editing.

Conflicts of interest

The authors declare that they have no known competing financial interests or personal relationships that could have appeared to influence the work reported in this paper.

Data availability

The data that support the findings of this study are available from the corresponding author upon reasonable request. All experimental data, including the characterization of e-GO nanosheets, epoxy/CSB-eGO nanocomposites, and the mechanical and anti-corrosive properties of epoxy/CSB-eGO nanocomposites, are included in the manuscript.

Acknowledgements

This research was supported by the National Foundation for Science and Technology Development (NAFOSTED) under grant number NCUD.02-2024.21. We also would like to acknowledge the A&A Green Phoenix Group JSC through Financial Supports for Purchasing Research Equipments of Key Research Group (NEB Lab). The authors would like to acknowledge the supports for Raman and electrochemical measurements from NEB Lab (Phenikaa University).

References

1 H. Q. Pham and M. J. Marks, Epoxy resins, *Ullmann's Encyclopedia of Industrial Chemistry*, 2000.
2 F.-L. Jin, X. Li and S.-J. Park, Synthesis and application of epoxy resins: A review, *J. Ind. Eng. Chem.*, 2015, **29**, 1–11.

3 T. Liu, *et al.*, Preparation of fully epoxy resin microcapsules and their application in self-healing epoxy anti-corrosion coatings, *Prog. Org. Coat.*, 2024, **188**, 108247.
4 J. Ma, *et al.*, Degradation and lifetime prediction of epoxy composite insulation materials under high relative humidity, *Polymers*, 2023, **15**(12), 2666.
5 Q. Cao, *et al.*, Evaluation of epoxy-based coating degradation under thermal insulation at elevated temperatures on different steel substrates, *Prog. Org. Coat.*, 2023, **180**, 107544.
6 N. A. Bratasyuk, A. V. Latyshev and V. V. Zuev, Water in epoxy coatings: Basic principles of interaction with polymer matrix and the influence on coating life cycle, *Coatings*, 2023, **14**(1), 54.
7 H. Zargarnezhad, *et al.*, Water transport through epoxy-based powder pipeline coatings, *Prog. Org. Coat.*, 2022, **168**, 106874.
8 J. Parameswaranpillai, *et al.*, *Epoxy Composites*, Wiley Online Library, 2021.
9 J. Zhang, *et al.*, Advances in Toughening Modification Methods for Epoxy Resins: A Comprehensive Review, *Polymers*, 2025, **17**(9), 1288.
10 D. Morselli, *et al.*, Epoxy networks reinforced with TiO_2 generated by nonhydrolytic sol–gel process: A comparison between in situ and ex situ syntheses to obtain filled polymers, *Polym. Eng. Sci.*, 2015, **55**(7), 1689–1697.
11 F. A. Gonçalves, *et al.*, Influence of fillers on epoxy resins properties: a review, *J. Mater. Sci.*, 2022, **57**(32), 15183–15212.
12 A. Balaskas, *et al.*, Improving the corrosion protection properties of organically modified silicate–epoxy coatings by incorporation of organic and inorganic inhibitors, *Prog. Org. Coat.*, 2011, **72**(4), 653–662.
13 I. Rafique, A. Kausar and B. Muhammad, Epoxy resin composite reinforced with carbon fiber and inorganic filler: Overview on preparation and properties, *Polym.-Plast. Technol. Eng.*, 2016, **55**(15), 1653–1672.
14 M. R. Ahmed, L. Maio and P. Potluri, Graphene-enhanced epoxy composites: A comprehensive review of dispersion mechanisms, processing strategies, property optimization, characterization and sustainable innovations, *Prog. Aerosp. Sci.*, 2025, **158**, 101142.
15 M. Shahbazi, *et al.*, Dispersion strategies of nanomaterials in polymeric inks for efficient 3D printing of soft and smart 3D structures: A systematic review, *Adv. Colloid Interface Sci.*, 2024, **333**, 103285.
16 R. M. Neves, *et al.*, Toughening epoxy resin with liquid rubber and its hybrid composites: A systematic review, *J. Polym. Res.*, 2022, **29**(8), 340.
17 S. Sprenger, Epoxy resins modified with elastomers and surface-modified silica nanoparticles, *Polymer*, 2013, **54**(18), 4790–4797.
18 R. A. Pearson and A. F. Yee, Toughening mechanisms in thermoplastic-modified epoxies: 1. Modification using poly(phenylene oxide), *Polymer*, 1993, **34**(17), 3658–3670.
19 S. Chung, *et al.*, Evaluation for micro scale structures fabricated using epoxy-aluminum particle composite and its application, *J. Mater. Process. Technol.*, 2005, **160**(2), 168–173.
20 E. Varga, *et al.*, Novel insights into the morphological effects of micron-scale inorganic fillers on polyethylene composites, *Compos. Commun.*, 2025, **56**, 102394.
21 A. A. Azeez, *et al.*, Epoxy clay nanocomposites – processing, properties and applications: A review, *Composites, Part B*, 2013, **45**(1), 308–320.
22 Z. Ahmadi, Epoxy in nanotechnology: A short review, *Prog. Org. Coat.*, 2019, **132**, 445–448.
23 X. Shi, *et al.*, Effect of nanoparticles on the anticorrosion and mechanical properties of epoxy coating, *Surf. Coat. Technol.*, 2009, **204**(3), 237–245.
24 H. Kim and C. W. Macosko, Processing-property relationships of polycarbonate/graphene composites, *Polymer*, 2009, **50**(15), 3797–3809.
25 J. Reif, *et al.*, Enhanced mechanical properties of nanocomposites at low graphene content, *ACS Nano*, 2009, **3**(12), 3884–3890.
26 J. Wei, T. Vo and F. Inam, Epoxy/graphene nanocomposites – processing and properties: a review, *RSC Adv.*, 2015, **5**(90), 73510–73524.
27 T. Fujigaya, Development of polymer-wrapping methods for functionalization of carbon materials, *Polym. J.*, 2023, **55**(3), 181–191.
28 J. Wu, G. Ji and Q. Wu, Preparation of epoxy/ZrO_2 composite coating on the Q235 surface by electrostatic spraying and its corrosion resistance in 3.5% NaCl solution, *RSC Adv.*, 2022, **12**(17), 10625–10633.
29 M. Cui, *et al.*, Polydopamine coated graphene oxide for anticorrosive reinforcement of water-borne epoxy coating, *Chem. Eng. J.*, 2018, **335**, 255–266.
30 F. Hussain, *et al.*, Polymer-matrix nanocomposites, processing, manufacturing, and application: an overview, *J. Compos. Mater.*, 2006, **40**(17), 1511–1575.
31 B. Bittmann, F. Haupert and A. K. Schlarb, Preparation of TiO_2/epoxy nanocomposites by ultrasonic dispersion and their structure property relationship, *Ultrason. Sonochem.*, 2011, **18**(1), 120–126.
32 M. Mehrabi Kooshki and A. Jalali-Arani, High performance graphene oxide/epoxy nanocomposites fabricated through the solvent exchange method, *Polym. Compos.*, 2018, **39**(S4), E2497–E2505.
33 J. Wei and F. Inam, Processing of epoxy/graphene nanocomposites: effects of surfactants, *J. Polym. Sci. Appl.*, 2017, **1**(1), 1–7.
34 A. A. Javidparvar, R. Naderi and B. Ramezanzadeh, Non-covalently surface modification of graphene oxide nanosheets and its role in the enhancement of the epoxy-based coatings physical properties, *Colloids Surf., A*, 2020, **602**, 125061.
35 V.-S. Vo, *et al.*, Crucial role of covalent surface functionalization of clay nanofillers on improvement of the mechanical properties of bioepoxy resin, *ACS Sustain. Chem. Eng.*, 2019, **7**(18), 15211–15220.
36 J.-B. Wu, *et al.*, Raman spectroscopy of graphene-based materials and its applications in related devices, *Chem. Soc. Rev.*, 2018, **47**(5), 1822–1873.

37 V. Gupta, *et al.*, Higher oxidation level in graphene oxide, *Optik*, 2017, **143**, 115–124.
38 D. R. Dreyer, *et al.*, The chemistry of graphene oxide, *Chem. Soc. Rev.*, 2010, **39**(1), 228–240.
39 F. Osterholtz and E. Pohl, Kinetics of the hydrolysis and condensation of organofunctional alkoxysilanes: a review, *J. Adhes. Sci. Technol.*, 1992, **6**(1), 127–149.
40 C. May, *Epoxy Resins: Chemistry and Technology*, Routledge, 2018.
41 K. Unnikrishnan and E. T. Thachil, Toughening of epoxy resins, *Des. Monomers Polym.*, 2006, **9**(2), 129–152.
42 M. Li, Z. G. Zhang and Z. J. Sun, Contact angle of epoxy resin measured by capillary impregnation and the Wilhelmy technique, *Polym. Polym. Compos.*, 2006, **14**(3), 251–259.
43 A. Trentin, *et al.*, Electrochemical characterization of polymeric coatings for corrosion protection: A review of advances and perspectives, *Polymers*, 2022, **14**(12), 2306.